MICROMECHANICAL CHARACTERISTICS OF THE SURFACE LAYER OF 45 STEEL AFTER ELECTRIC-SPARK TREATMENT

V. M. Holubets',[1,2] **M. I. Pashechko,**[3] **J. Borc,**[3] **and M. Barszcz**[3]

UDC 620.198

We analyze the principal micromechanical characteristics of the surface layers of 45 steel with electric-spark coatings, namely, their microhardness, microplasticity (creep), Young's modulus, elastic and relaxation properties, elasticity of microstrains, and the changes in the contact stiffness.

Keywords: electric-spark coating, nanoindentation, nanoscratching, micromechanical characteristics.

Introduction

As a major task of mechanical engineering, we can mention the necessity of increasing the reliability and durability of machine components, mechanisms, and cutting tools. In this case, an important applied problem is to guarantee the realization of conditions of steady-state friction and wear in elements of tribojoints and the stability of their operation.

The technology of electric-spark alloying (ESA) is now extensively used in the industry due to the possibility of transfer of any conducting materials onto the hardened surface, high strength and adhesion of the hardened surface layer of the metal, local deposition of electric-spark coatings (ESC) without noticeable deformation, the absence of heating of the treated surface, and low energy consumption. For the efficient application of ESA, it is important to develop and master new electrode materials (today, these are mainly titanium–cobalt and tungsten–cobalt hard alloys, and graphite; in some cases, also chromium, white cast iron, etc.). The restoration of the sizes of components is also performed by the ESA method, as a rule, with the help of electrodes made of materials similar in their physicomechanical properties to the material of the product.

In the process of friction, the contacting surfaces are subjected to various mechanical and thermal actions, which strongly affects both the structural changes in the surface layer and the tribotechnical parameters of friction couples. The tribological behaviors of the components are determined by the physicomechanical properties of the surface layers with a thickness of up to 0.1 mm. Note that the contact processes are localized in these layers [1]. Under the conditions of friction, the surface microasperities suffer the action of stresses in different directions. These stresses vary from compression to tension and damage the surface [2]. The fracture resistance and the character of damages are determined, first of all, by the mechanical characteristics of the surface layers and the works of elastic and plastic deformation of the microasperities. These quantities may undergo significant changes under the influence of the components of the medium [3, 4].

The micromechanical characteristics of thin surface layers in micro- and submicrovolumes can be evaluated either by the dynamic nanoindentation with recording of the kinetic diagrams of indentation [5, 6] or by using

[1] Ukrainian National Forestry University, Lviv, Ukraine.

[2] Corresponding author; e-mail: golubets.volodymyr@gmail.com.

[3] Lublin University of Technology, Lublin, Poland.

Table 1

Components of the Charge for PP-NP-PD 80Kh20R3T Powder Wires (wt.%)

Components of the charge	Fe	Cr	B	Ti
FKhB-2	50	30	20	–
FKh100	35	65	–	–
Ti-1	70	–	–	30

the scratch method [7]. The works on the influence of thermal treatment of steel [8] after electrolytic hydrogenation [9] and overlaying [10] of the surfaces with deposited protective coatings [11, 12] were devoted to investigations of this kind.

The aim of the present work is to determine some micromechanical characteristics of the surface layer of 45 steel with the use of powder wires I (PD 80Kh20R3T) and II (combined) as electrodes for the procedure of ESA. The investigations were carried out on microsections.

Methods of Investigations

Materials of the Electrodes and the ESA Modes. A combined electrode was made of MPG-7 graphite 6 mm in diameter. In this electrode, we drilled an internal hole 3.2 mm in diameter and inserted an 80Kh20R3T powder wire (PW). The length of the electrode was equal to 30 mm.

The shell of the powder wire was made of 08kp low-carbon steel and filled with a powder mixture based on ferroalloys (Table 1). The chemical composition of the powder wire was as follows: 20 wt.% Cr, 3 wt.% B, 1 wt.% Ti, 0.8 wt.% C, balance Fe. The commercial PP-AN 170 self-protecting powder wires (PP-Np-PD 80Kh20R3T) $\varnothing$ 3.2 were produced by the "ELNA" LLC Scientific-Production Firm (Kyiv, Ukraine).

The ESC were deposited with the help of an "Elitron" installation for ESA produced by the experimental plant at the Institute for Applied Physics of the Academy of Sciences of Moldova, which consists of a generator and a manually operated vibrator, in the ninth mode of alloying (the third mode of capacitance and voltage; the capacitance of the storage battery of capacitors is equal to 630 μF; the amplitude of pulses of the storage capacitors is 58 V, the working current is 9 A, and the frequency of pulses is 100 Hz).

The procedure of electric-spark alloying is based on the application of the phenomena accompanying the process of abrupt release of the electric energy and is characterized by the high temperature of the spark channel and the ionization of the interelectrode space. In connection with the fact that, this process is characterized by the presence of short pulses of electric current with durations of 10^{-3}–10^{-5} sec, the efficient heat removal on the electrodes (from the site of discharge to the treated surface) cannot be guaranteed by the thermal conductivity of the metal. Hence, small volumes of the surface layers of the metal are subjected to abrupt temperature fluctuations from the boiling point of the metal on the electrodes down to temperature of several tens of degrees [13].

Nanoindentation. The nanoindentation tests of the investigated materials were carried out with the help of an Ultra Nano Hardness Tester (UNHT) by using a Berkovich diamond indenter at room temperature.
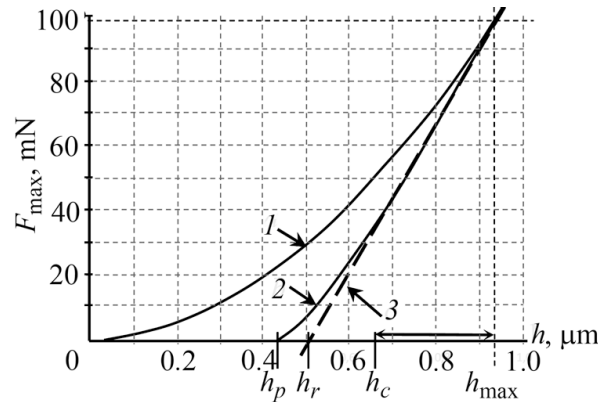
Fig. 1. Loading diagram under the conditions of dynamic indentation: h_c is the depth of penetration of the indenter for F_{max}; h_r is the depth of depression computed according to the contact stiffness of the material (3) and h_p is the depth of depression that remains in the coating after removal of the force F; (1) and (2) are areas under the branches of loading and unloading, respectively.

The mechanical characteristics of the surface layers were found by the method of dynamic indentation [5]. This method is based on the automatic recording of the loading diagram $F = f(h)$, where F is the load on the indenter and h is the depth of its penetration into the surface of the investigated material (Fig. 1). The main advantage of the method is that the hardness is determined at the time of maximum penetration of the tip (h_{max}), i.e., prior to the onset of the elastic recovery of the material. Thus, this diagram gives information about the work required for the indenter to overcome the resistance of the material W_{plast} (curve 1) and the work of recovery of its characteristics by the material W_{elast} (curve 2). The degree of plasticity of the surface is determined according to these results by the formula

$$\varepsilon = (W_{plast} - W_{elast})/W_{plast}$$

and h_r is found by using the contact stiffness S (curve 3) according to the formula $\varepsilon(h_{max} - h_r)$.

The kinetic diagrams of indentation make it possible to study the micromechanical characteristics of the surface layers of materials: their microhardness, microplasticity (creep), elastic and relaxation properties, and the variations in the contact stiffness.

The main improvements of the installation are as follows: a new tip and a system of reference recording inserted in the Ultra Indenter Head, which uses the active upper ratios of signals in the course of measurements under very low loads (lower than 0.01 N) and makes it possible to measure the depths and loads; the absence of temperature effect; the presence of feedback under the loop control of loading realized with the help of control and indenter systems, low thermal drift, high resonance frequency, and new electronic design. The nanoindentation tests were performed with the help of a load regulator in the linear mode for a rate of loading and unloading of 100 mN/min and a holding time of 20 sec. Each specimen was measured under a maximum load of 50 mN. We carried out five measurements on different areas of the coating and computed the mean values of hardness and Young's modulus. The images of the chosen indents were obtained with the help of optical microscopy.

The identified module H was found according the standard relation

$$H = \frac{F_{max}}{A}, \tag{1}$$

where F_{max} is the maximum testing load and A is the projected contact area.

The modulus of elastic deformation E^* is determined by the Oliver–Pharr method as follows [14]:

$$E^* = \frac{1}{\dfrac{1}{E_r} - \dfrac{1 - \nu_i^2}{E_i}}, \tag{2}$$

where E_r is the modulus of elasticity of the indenter (1141 GPa for diamond) and ν is Poisson's ratio for the indenter (0.07 for diamond).

We calculate the modulus E_r as follows:

$$E_r = \frac{\sqrt{\pi} S}{2\beta \sqrt{A_p(h_c)}}, \tag{3}$$

where β is the geometric coefficient of the indenter ($\beta = 1.034$ for the triangular shape); h_c is the depth of penetration of the indenter at $F_{\max}$, and S is the contact stiffness determined by the value of the derivative under the peak load:

$$S = \left(\frac{dF}{dh}\right)_{\max}. \tag{4}$$

Young's modulus E_{IT} is determined from the expression for E^* with the use of Poisson's ratio (ν_s)

$$E_{IT} = E^*(1 - \nu_s^2). \tag{5}$$

The typical values of ν_s are 0.1–0.3 for ceramics, 0.2–0.4 for metals, and 0.3–0.4 for polymers.

The micromechanical properties of the surface layers were measured according to the norms [15].

Scratch Testing. The investigated materials were tested with the use of a Nano-Scratch Tester (NST) produced by the CSM Instruments and equipped with a rod whose tip has the form of a spheroconical diamond indenter with a radius of $2\ \mu m$. The investigations were carried out at room temperature in the mode of repeated scanning (preliminary scanning–scratching–after scanning), which enabled us to determine the profile of P and the depths of scratching D_1 and D_2. Scratching tests were performed in a progressive loading mode with the following parameters: the initial test load was 0.2 mN, the maximum test load was 20, 25, 50, and 100 mN, the rate of its change was 2 mN/sec, and the length of a scratch was 0.8 mm. The load in tests of preliminary scanning and after scanning was 0.2 mN. The tests were repeated at least three times for each specimen, which allowed us to get the mean values of the required parameters [7].

Results of Investigations and Their Analysis

Nanoindentation. We studied the micromechanical characteristics of the ESC whose absolute values are presented in Table 2. The Young's moduli (E_{IT}, E_r, and E^*), creep C_{IT}, and hardnesses H_{IT} and $HV_{0.02}$ (Table 2) for the coatings obtained with the use of the powder wire II are higher than for the coatings deposited from powder wire I.

Table 2
Micromechanical Characteristics of the ESC

Characteristics / Electrode	H_{IT}, GPa	E_{IT}	E_r	E^*	C_{IT}, %	A_p, nm^2
		GPa				
Powder wire I	18.462	180.95	169.46	198.84	0.86	2708448.20
Powder wire II	24.958	207.86	190.47	228.42	0.97	2003599.44

Continuation of Table 2

W_{elast}	W_{plast}	W_{total}	η_{IT}, %	P	R	$HV_{0.02}$
	pJ					
4169.72	5168.76	9331.48	44.68	0.55	0.45	1709.8
4270.46	4127.42	8397.88	50.85	0.49	0.51	2311.4

Continuation of Table 2

F_{max}, mN	h_{max}, nm	S, mN/nm	h_c	h_r	h_p	m	ε
			nm				
50	492.69	0.3254	366.71	339.02	319.74	1.13	0.82
50.01	444.232	0.3146	313.23	285.26	267.19	1.11	0.82

The works of the forces of elastic deformation W_{elast} and the elastic part of the diagram of η_{IT} are larger for the coating obtained from the powder wire II, whereas the work of plastic deformation W_{plast} is larger for the coating obtained from the powder wire I. The coefficient P ($P = W_{plast}/W_{total}$) that characterizes the plasticity of the material is higher for the coating deposited from the powder wire I. The coefficient R ($R = W_{elast}/W_{total}$) is the relative contribution of the relaxation processes in the stage of unloading and the relaxation ability of the material is higher for the coating deposited from the powder wire II.

The Vickers microhardness $HV_{0.02}$ is higher for the coating deposited from the powder wire II. The contact stiffness S, the maximum depth of penetration of the indenter h_{max}, the depth of depression caused by the indenter h_c for F_{max}, the depth of depression h_r computed according to the contact stiffness of the material, the depth of depression h_p that remains in the material when the force F is removed, the parameter m of adjustment of the force to the loading curve are higher for the coating obtained from the powder wire I. The values of the geometric constant ε are identical for both investigated coatings.

Since there exists a clear difference between the values of the micromechanical characteristics of the ESC obtained from the powder wires I and II, we present (Figs. 2 and 3) the diagrams of changes in the load and
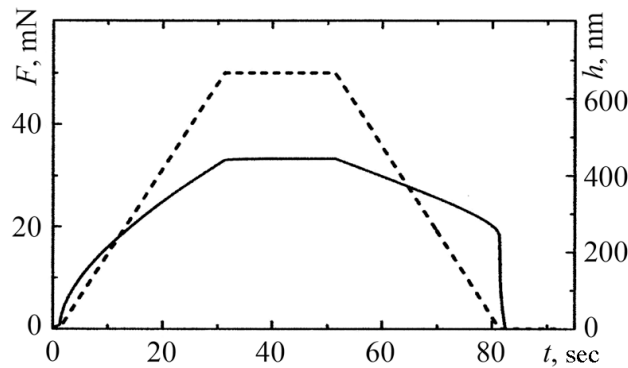
Fig. 2. Diagrams of changes in the load and in the depth of penetration for the coating obtained from the powder wire II; the dashed line corresponds to F and the solid line corresponds to h.
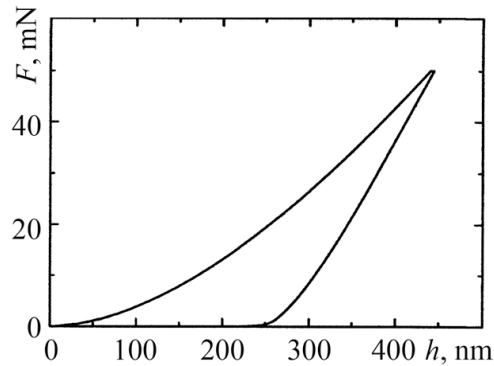

Fig. 3. Kinetic diagram of continuous microindentation by an indenter for the coating obtained from the powder wire II.
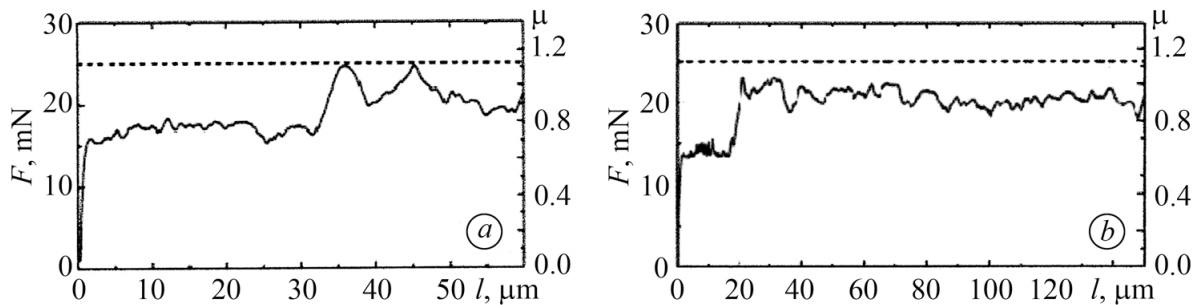

Fig. 4. Scratch testing of the coatings deposited from the powder wires I (a) and II (b) under a load on the indenter $F_n = 25$ mN; the dashed line corresponds to F_n and the solid line corresponds to μ; l is the length of the nanoscratch.

in the depth of penetration of the indenter, as well as the kinetic diagram of continuous microindentation for the coating deposited from the powder wire II.

Coating obtained from the powder wire I. Under a load on the indenter of 25 mN, the friction coefficient varies within the range 0.7–1.15 (Fig. 4a). At the same time, under loads of 50 and 100 mN, it varies within the range 0.75–0.90.
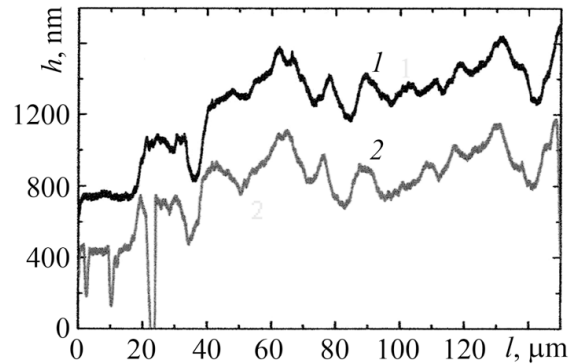
Fig. 5. Depth of penetration (1) and the recovery depth (2) in the course of scratch testing of the coating deposited from the powder wire II under a load on the indenter of 25 mN: l is the length of the nanoscratch.
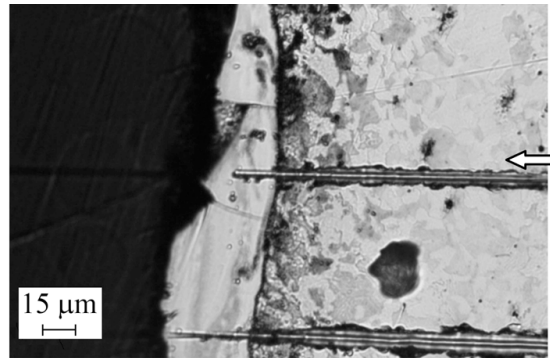

Fig. 6. Microstructure of the scratch-tested coating deposited from the powder wire II under a load on the indenter of 25 mN.

Under a load of 25 mN, the depth of penetration of the indenter in the coating is ~ 900 nm. The recovered depth (after removal of the load) is ~ 300 nm (the length of indentation is up to 0.06 mm). The depth of penetration (900–1400 nm) of the indenter and the recovered depth (150–500 nm) in 45 steel are larger. Under a load on the indenter of 50 mN, these quantities are ~ 1600 and ~ 250 nm, respectively. At the same time, under a load of 100 mN, they are ~ 750 and ~ 550 nm, respectively. In 45 steel, under a load of 50 mN, the depth of penetration of the indenter is 1600–2400 nm and the recovered depth can be as large as up to 500–750 nm, whereas under a load of 100 mN, they are equal to 3000–3750 and 1000 nm, respectively.

Coating obtained from the powder wire II. Under a load on the indenter of 25 mN, the friction coefficient varies within the range 0.8–1.0 (Fig. 4b). At the same time, under loads of 50 and 100 mN, it varies within the ranges 0.7–0.8 and 0.85–0.92, respectively.

The depth of penetration of the indenter in the coating under a load of 25 mN is ~ 750–1100 nm and the recovered depth (after removal of the load) is ~ 100–700 nm (the length of indentation is up to 0.01 mm). The depth of penetration (1200–1700 nm) of the indenter and the recovered depth (750–1200 nm) in 45 steel are larger (Fig. 5). Under a load on the indenter of 50 mN, these quantities are, respectively, ~ 700 and ~ 500 nm and, under a load of 100 mN, they are ~ 750 and ~ 550 nm. In 45 steel, under a load of 50 mN, the depth of penetration of the indenter is 1500–2500 nm and the recovered depth is 750–1000 nm, whereas under a load of 100 mN, they are equal to 3000–4500 nm and 750 nm, respectively.

The microstructure of the coating subjected to scratch testing is shown in Fig. 6.

CONCLUSIONS

The procedure of electric-spark alloying of 45 steel performed with the help of electrodes made of powder wires in the indicated modes strongly affects the surface engineering in the course of deposition of the ESC. We revealed a noticeable difference between the parameters of micro- and submicrovolumes of the surface layer of ESC depending on the procedure of alloying (with electrode I or with the combined electrode II); the values obtained by using electrode II are much higher. As important characteristics of the micromechanical properties of materials for triboengineering in the evaluation of the regularities and mechanisms of tribological behavior of the ESC in the course of friction and wear, we can mention: the works of forces of elastic W_{elast} and plastic W_{plast} deformation; the coefficients P for plasticity and R for the relaxation ability of the material; the hardnesses H_{IT} and $HV_{0.02}$; Young's modulus E_{IT}, which reflects the increase in the strength of the coating and, hence, the decrease in the depth of penetration of the indenter in the course of nanoindentation, and the friction coefficient μ. The numerical values of the micromechanical characteristics can be useful for the development of new engineering approaches aimed at the evaluation of strength, stiffness, durability, and the stress-strain states of the tribomaterials for machine components operating under conditions of contact interaction.

REFERENCES

1. I. I. Berkovich and D. G. Gromakovskii, *Tribology, Physical Foundations, Mechanics, and Engineering Applications* [in Russian], Samara State Technical University, Samara (2000).
2. J. W. Jones and J. J. Wert, "The effects of gaseous environments on the wear of commercial purity titanium," *Wear,* **32**, 363–377 (1975).
3. T. Sasada, K. Hiratsuka, and H. Saito, "Adsorption of surrounding gas molecules on pure metal surfaces during wear processes," *Wear,* **135**, 251–264 (1990).
4. M. M. Student, V. M. Dovhunyk, M. D. Klapkiv, V. M. Posuvailo, V. V. Smyrko, and A. P. Kytsya, "Tribological properties of combined metal-oxide-ceramic layers on light alloys," *Fiz.-Khim. Mekh. Mater.,* **48**, No. 2, 55–64 (2012); *English translation: Mater. Sci.,* **48**, No. 2, 180–190 (2012).
5. Yu. I. Golovin, *Nanoindentation and Its Possibilities* [in Russian], Mashinostroenie, Moscow (2009).
6. S. I. Bulychev, V. P. Alekhin, and M. Kh. Shorshorov, "Investigation of the physicomechanical properties of materials in the near-surface layers and in microvolumes by the method of continuous forcing of the indenter into a material (a survey)," *Fiz. Khim. Obrab. Mater.,* No. 5, 69–81 (1979).
7. P. J. Blau, "Scratch adhesion testing," in: *Lab Handbook of Scratch Testing,* Chapter 7, *Blue Rock Tech. Publ.,* Oak Ridge (2002), pp. 7.1–7.15.
8. V. V. Shevelya, A. S. Trytek, V. P. Oleksandrenko, and Yu. S. Sokolan, "Structural and rheological mechanisms of decreasing the levels of dynamic stresses and strain hardening of the friction contact," *Probl. Trybolog.,* No. 1, 6–15 (2010).
9. V. A. Vinar, M. Ya. Holovchuk, Kh. B. Vasyliv, and V. I. Zakiev, "Changes in the micromechanical properties of the surface layers of Fe, Cu, and Ti after electrolytic hydrogenation," *Nauk. Notat.,* **1,** No. 41, 38–44 (2013).
10. A. A. Vojtovych, H. V. Pokhmurs'ka, M. M. Student, and O. Z. Student, "Microstructure and abrasive-wear resistance of the vibration-deposited metal of core wires of the basic Fe–Cr–B system," *Fiz.-Khim. Mekh. Mater.,* **52**, No. 3, 63–68 (2016); *English translation: Mater. Sci.,* **52**, No. 3, 365–370 (2016).
11. G. G. Gorokh, M. I. Pashechko, J. T. Borc, A. A. Lozovenko, I. A. Kashko, and A. I. Latos, "Matrix coatings based on anodic alumina with carbon nanostructures in the pores," *Appl. Surf. Sci.,* **433**, 829–835 (2018).
12. M. M. Student, V. V. Smyrko, M. D. Klapkiv, I. M. Lyasota, and L. N. Dobrovol'ska, "Evaluation of the mechanical properties of combined metal-oxide-ceramic layers on aluminum alloy," *Fiz.-Khim. Mekh. Mater.,* **50**, No. 2, 116–121 (2014); *English translation: Mater. Sci.,* **50**, No. 2, 290–295 (2014).
13. G. P. Ivanov, *Technology of Electric-Spark Hardening for Tools and Machine Components* [in Russian], Mashgiz, Moscow (1961).
14. W. C. Oliver and G. M. Pharr, "An improved technique for determining hardness and elastic modulus using load and displacement sensing indentation experiments," *J. Mater. Res.,* **7**, No. 6, 1564–1583 (1992).
15. *Norma PN-EN ISO 14577-1: 2005. Instrumentalna Próba Wciskania Wgłębnika do Okreslania Twardości i Innych Własności Materiałów. Część I. Metoda Badania,* Publ. on 13.07.2005.